Optical Anisotropy of Flagellin Layers: In Situ and Label-Free Measurement of Adsorbed Protein Orientation Using OWLS

ARTICLE *in* ANALYTICAL CHEMISTRY · APRIL 2013

Impact Factor: 5.64 · DOI: 10.1021/ac3034322 · Source: PubMed

7 AUTHORS, INCLUDING:

Jeremy Ramsden
Collegium Basilea (Institute of Advanced Stud…
230 PUBLICATIONS **5,921** CITATIONS

SEE PROFILE

Ferenc Vonderviszt
University of Pannonia, Veszprém
66 PUBLICATIONS **1,788** CITATIONS

SEE PROFILE

Robert Horvath
Institute of Technical Physics and Materials Sc…
77 PUBLICATIONS **1,043** CITATIONS

SEE PROFILE

analytical chemistry

Article

pubs.acs.org/ac

Optical Anisotropy of Flagellin Layers: In Situ and Label-Free Measurement of Adsorbed Protein Orientation Using OWLS

Noemi Kovacs,[†] Daniel Patko,[†,‡] Norbert Orgovan,[†] Sandor Kurunczi,[†] Jeremy J. Ramsden,[§,∥] Ferenc Vonderviszt,[†,‡] and Robert Horvath*[,†]

[†]Department of Photonics, MTA TTK MFA, Budapest, Hungary

[‡]Bio-Nanosystems Laboratory, Research Institute of Chemical and Process Engineering, Faculty of Information Technology, University of Pannonia, Veszprém, Hungary

[§]Collegium Basilea (Institute of Advanced Study), Basel, Switzerland

[∥]Cranfield University, Bedfordshire, United Kingdom

ABSTRACT: The surface adsorption of the protein flagellin was followed in situ using optical waveguide lightmode spectroscopy (OWLS). Flagellin did not show significant adsorption on a hydrophilic waveguide, but very rapidly formed a dense monolayer on a hydrophobic (silanized) surface. The homogeneous and isotropic optical layer model, which has hitherto been generally applied in OWLS data interpretation for adsorbed protein films, failed to characterize the flagellin layer, but it could be successfully modeled as an uniaxial thin film. This anisotropic modeling revealed a significant positive birefringence in the layer, suggesting oriented protein adsorption. The adsorbed flagellin orientation was further evidenced by monitoring the surface adsorption of truncated flagellin variants, in which the terminal protein regions or the central (D3) domain were removed. Without the terminal regions the protein adsorption was much slower and the resulting films were significantly less birefringent, implying that intact flagellin adsorbs on the hydrophobic surface via its terminal regions.

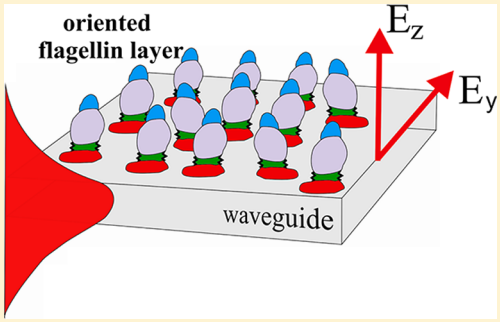

The adsorption of proteins at solid−liquid interfaces has important roles in nature, medicine, and industry. Therefore, achieving understanding of the adsorption behavior of proteins, the main driving forces and their dependences on peptide and substrate material composition not only is crucial for the deep understanding of basic biological processes and the nature of life but also has significant importance for the development of contemporary technologies.[1−3]

Many experimental configurations have been developed to investigate the adsorption of proteins.[4] These include techniques based on labeling using fluorescent or radioactive markers,[3] which are quite useful to sensitively measure the adsorbed amount of biomolecules. But, the markers necessarily perturb the system under study and care should therefore be taken when interpreting the results. Recently, much attention has turned to label-free techniques in which the protein itself gives a signal because of its inherent mass or refractive index.[3−7] Such techniques include quartz crystal microbalance (QCM) and acoustic wave sensors based on mass sensing and ellipsometry, surface plasmon resonance (SPR), coupled plasmon-waveguide resonance (CPWR) spectroscopy,[8] optical waveguide lightmode spectroscopy (OWLS), and dual polarization interferometry (DPI) employing refractive index sensing and polarized visible attenuated total reflection (ATR) spectroscopy, which relies on the protein's native chromophore.[9,10] Among these, the optical systems are generally the most sensitive, with reported surface mass detection limits in the 0.1−10 pg/mm^2 range.[11−16] Using optical microcavities the label-free detection of even a single molecule has been reported.[17] This high sensitivity and excellent time resolution of the measurements opened the way to experimentally investigate the kinetics of protein adsorption on various surfaces without using any labeling,[2,18,19] that is, without unnecessarily perturbing the system.

Although the kinetics are thereby well investigated,[20,21] much less is known about the structure of the adsorbed protein layers, mainly due to the lack of experimental techniques to sensitively measure such structure at the nanometer scale in aqueous environments and the lack of optical theories to correctly interpret the experimental data. In fact, the homogeneous and isotropic thin film approximation is generally used to interpret the experimental data to give structural information. Notable exceptions are the techniques of polarized visible ATR spectroscopy and polarized total internal reflection (TIR) spectroscopy,[9,10,22−24] which enable anisotropic optical constants and orientation to be determined, using a native chromophore or fluorophore of the proteins. These single-mode planar optical waveguide based techniques, introduced, and theoretically investigated by Mendes and Saavedra,[9,23] are

Received: November 26, 2012
Accepted: April 30, 2013
Published: April 30, 2013

   dx.doi.org/10.1021/ac3034322 | *Anal. Chem.* 2013, 85, 5382−5389

used to probe changes in the imaginary part of the waveguide effective refractive index because of the presence of an adlayer. For example, Saavedra and co-workers investigated adsorbed cytochrome c films using these techniques.[25,26] Tollin and co-workers also extensively applied anisotropic optical models to characterize various biological films using CPWR.[27−30] Another fairly recent development is to use FTIR to determine the orientation of adsorbed proteins,[31] but there are severe limitations on the range of substrates that can be used, and the technique is not very sensitive for measuring the number of adsorbed molecules.

Among the label-free and in situ methods the planar optical waveguide-based techniques are especially promising candidates to sensitively measure the intrinsic structure of biological films, even at the subnanometer scale, using evanescent optical waves. In contrast to SPR, these are not single, but at least dual mode techniques. This means that they are capable of determining not only the adsorbed protein amount,[4] but two or more independent experimental parameters structurally characterizing the layer.[27−30,32,33]

In the present work, we use OWLS to monitor adsorbed protein orientation. OWLS probes changes in the real part of the waveguide effective refractive index and has never been applied before to investigate oriented protein adsorption. Unlike DPI, OWLS can potentially use more than two modes, concomitantly increasing the number of structural parameters obtainable from the measurements,[34−36] while retaining all the other advantages of optical methods.

Even if a compact layer assembled from nanoscale objects can be treated as homogeneous at optical wavelengths,[37] the justification of the *assumption of isotropy* is not self-evident. Proteins can have significant intrinsic complexity and are generally far from spherical in shape; this is especially true for large multidomain proteins with a far from homogeneous distribution of electrostatically charged, polar and apolar residues.[38] As we will show in the present study, this characteristically different structure and composition of the various protein domains can cause oriented protein adsorption on solid surfaces. For an oriented adsorbed layer the assumption of optical isotropy cannot be expected to be valid, since the individual molecules are themselves neither homogeneous nor isotropic. Instead, we almost certainly have anisotropy (exceptions are likely to be fortuitous), implying different refractive indices parallel and perpendicular to the substrate. The structural ordering can be determined from the optical birefringence of the adsorbed layer in a completely label-free manner, as has already been done with, for example, supported lipid bilayer membranes,[27,35,39,40] which are known from other structural techniques such as X-ray diffraction (albeit applied to multiply stacked lipid bilayers) to be strongly anisotropic.

Our recent theoretical work to extend the capabilities of planar optical waveguide-based label-free methods showed that birefringence in the adsorbed layer leads to implausible refractive index (n) and thickness (d) values when the generally applied isotropic layer model is used.[40] Nevertheless, even using the isotropic model for an anisotropic film, we have shown that the adsorbed protein mass per unit area calculated from n and d is accurate to within typical experimental uncertainty.[40] It was further shown that the obviously unrealistic values (when compared with independent structural data, such as the molecular dimensions determined from X-ray crystallography) of the optogeometrical parameters can reveal the sign of the layer birefringence. For example, overestimated refractive index values originate from *negative* birefringence in the adsorbed layer, but negative or very "noisy" quasi-isotropic thicknesses are linked to *positive* birefringence.[40] In another work, treating the adsorbed layer as optically anisotropic revealed a significant anisotropic adsorption−desorption hysteresis in self-assembled mucin films,[41] mucin also being a complex biomacromolecule. The inferred structure of the glycoprotein layer was in full agreement with its biological role of boundary lubrication.[42,43]

In the present study, we use the previously developed methodology[40,41] to investigate the adsorption and intrinsic layer structure of surface-adsorbed flagellin thin films. This protein is the main building block of bacterial flagellar filaments in many species, including *Salmonella typhimurium* and *Escherichia coli*.[44] Flagellin has a complex structure containing well-folded protein domains and intrinsically disordered regions as well.[45]

Salmonella flagellin is composed of 494 amino acids. Proteolytic experiments and NMR studies revealed that both terminal regions of the molecule, comprising approximately the first 65 and the last 45 residues, are highly flexible without having an ordered tertiary structure in the monomeric form.[46,47] The central portion of the amino acid sequence, residues 66−450 (the F40 fragment), forms compact domains. The disordered terminal regions of flagellin are not completely unstructured but contain unstable α-helical secondary structural elements. These regions possess heptad repeats of hydrophobic amino acid residues, a characteristic of amphipathic helices that readily form α-helical coiled coils. The disordered regions become ordered upon filament formation into a largely α-helical domain.[50,51]

Electron cryomicroscopy and X-ray diffraction[51,52] studies have revealed the subunit structure within the filament. Polymeric flagellin consists of four linearly connected domains labeled D0, D1, D2, and D3, which are arranged from the inside to the outside of the filament. The disordered terminal regions are involved in D0 and partly in D1, forming long helical bundles, and their direct interaction is responsible for stabilizing the filament structure. A central segment from Tyr 190 to Val 283 makes up domain D3, which is exposed on the surface of flagellar filaments. D3 is a structurally independent part of flagellin; it is not essential for filament formation.[51]

The D3 domain is a good target for genetic engineering studies. It can be readily replaced by appropriate peptide sequences or foreign protein domains having specific molecular recognition properties or enzymatic activities without disturbing the polymerization ability.[48] Because of these exciting possibilities flagellin can find interesting applications in chemical or biological sensing, as well as in nanobiotechnology.[53]

The flagellin domains have rather different characteristics in terms of their surface hydrophobicities,[49] which is in close connection with the mechanism of flagellin assembly into flagellar filaments. This makes flagellin an ideal candidate for studying the roles of the various regions in the protein adsorption process because of the ease of systematically removing one or other of the protein domains. This possibility is explored in the present work by investigating the adsorption of flagellin and its truncated variants on an artificial hydrophobic surface using label-free optical waveguide lightmode spectroscopy. Employing our recently developed methodology to model the adsorbed thin layers as uniaxially anisotropic,[40]

dx.doi.org/10.1021/ac3034322 | Anal. Chem. 2013, 85, 5382−5389

the intrinsic layer structure of the protein films could be revealed, from which oriented flagellin adsorption was inferred.

PROTEIN SAMPLES AND WAVEGUIDE SURFACE PREPARATION

The isolation of flagellin (51.5 kDa) from *Salmonella typhimurium* and the preparation of its F40 fragment have been previously described.[46] Flagellin is made by heat-induced depolymerization of flagellar filaments, which means 15 min incubation at 65 °C. After heat treatment the solution was centrifuged through a 100 kDa filter (Millipore, UFC510008) to remove fragments of filaments still remaining in the sample. The F40 fragment (40 kDa) is obtained by mild tryptic digestion of flagellin to remove the disordered terminal regions of the molecule, which span the first 65 and the last 45 residues. The ΔD3_FliC flagellin mutant (42.5 kDa) deprived of the hypervariable D3 domain, containing residues 190−283, was prepared as decribed.[51] The proteins were dissolved at a final concentration of 1 mg/mL in phosphate-buffered saline (PBS, Sigma P4417) pH 7.4, 20 mM.

Pyrolyzed sol−gel SiO_2/TiO_2 planar optical waveguides (OW2400, MicroVacuum Ltd., Hungary), on a substrate of Schott AF45 optical glass, were cleaned for 3 min in chromic acid (Spektrum 3D), rinsed in Milli-Q ultrapure water, immersed into a KOH solution (1%), and then rinsed in copious amounts of ultrapure water to prepare the hydrophilic surfaces. The hydrophobic surfaces were made by covering the hydrophilic waveguides with hexamethyldisilazane (HMDS) using a toluene reflux, resulting in water contact angles of 90−95°. Prior to the optical measurements the waveguides were stored overnight in PBS.

INTEGRATED OPTICAL SCANNING

The prepared waveguides were placed into the head assembly of an OWLS 210 integrated optical scanner (MicroVacuum Ltd., Hungary) whereby a standard PEEK flow-through cuvette sealed with a Kalrez O-ring was positioned on top of the waveguide with the flow direction parallel to the grating lines. Using a 12 roller peristaltic pump (Ismatec, Reglo Digital) with 0.5 mm i.d. Tygon tubing, connected to the cuvette with 0.8 mm i.d. Teflon tubing, first pure buffer solution was pumped through the cuvette to observe any possible fluid leakage or air ingress (indicative of incorrect cuvette assembling). The fluidic system included a bubble trap just upstream of the cuvette. The leakage-free head assembly was then mounted on the OWLS scanner where a diagonally polarized He−Ne laser (632.816 nm) simultaneously excited the zeroth-order transverse electric (TE) and transverse magnetic (TM) modes of the waveguide. All subsequent solutions passed over the waveguide surface with a constant flow rate of 1.3 μL/s and every 18 s the scanner recorded the effective refractive indices (N_{TE} and N_{TM}) of the modes with a standard error of around 10^{-6}. The temperature was maintained at 25.0 °C at the head of the scanner using a Peltier-based temperature control system. The bulk refractive index (n_C) of the solutions were measured with a Rudolf refractometer at a wavelength of 633 nm.

During the propagation of the guided mode the evanescent optical waves of the mode extend into the waveguide cover medium and can monitor the deposited protein layer (see Figure 1). When the mode is propagating in the ***x*** direction the TE mode is sensitive to refractive index in the ***y*** direction (parallel to the surface of the waveguide) since its electric field vector has ***y*** components only.[39,40,54] Refractive index in the ***z*** direction (perpendicular to the surface) can be sensed by the TM polarization (see Figure 1). It should be noted that the TM polarization has not only ***z***, but also an ***x*** electric field vector component.[35,54] Supposing uniaxial symmetry in the adsorbed layer, the ***x*** and ***y*** directions can be treated as identical. In principle, refractive index variation parallel and perpendicular to the interface can be separated using two modes with different polarizations (see also Figure 1).

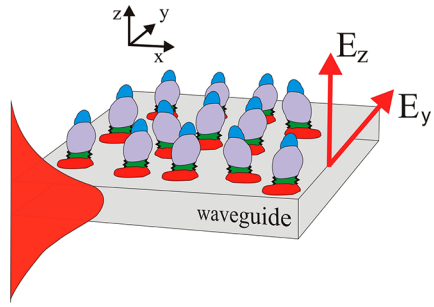

Figure 1. Optical guided mode traveling in the ***x*** direction detects the surface adsorbed protein layer through the exponentially decaying evanescent field of the mode. The evanescent wave extends into the protein film and senses the deposited molecules through their inherent refractive index (which differs from that of the medium). The orientation of the proteins in the adsorbed layer is detected by the ***y*** and ***z*** electric field components of the modes (see text).

RESULTS AND DISCUSSION

Effective Refractive Index Shifts Because of the Adsorbed Proteins. The protein adsorption experiments were always started by recording a stable (signal drift less than 10^{-8} effective refractive index units s^{-1}) baseline under buffer flow. The protein solution was made to flow into the cuvette (starting at zero time in all of the figures) resulting in an increase in the measured N_{TE} and N_{TM} values because of the adsorption of the proteins on the surface of the waveguide. Once the signals reached a new plateau, buffer solution was again pumped through the cuvette (washing) to remove any reversibly adsorbed proteins from the surface. The t (measurement epoch), N_{TE} and N_{TM} data sets were saved for subsequent analysis.

The resulting effective refractive index curves are shown in Figure 2. It is seen that in the presence of the flagellin solution the signal started to increase very rapidly and saturated in less than 5 min, indicating an extremely fast protein adsorption on the hydrophobic surface. In contrast, flagellin did not adsorb significantly on the hydrophilic surface (data not shown). It is important to note that the fast adsorption was also observed for the ΔD3_FliC fragment, but the adsorption of F40 was significantly slower (see Figure 2b,c). When the buffer solution was again made to flow into the cuvette the effective refractive indices started to decrease, but not back to the baseline.

Adsorbed Protein Mass Per Unit Area. From the measured effective refractive index data the time dependence of the adsorbed protein mass per unit area can be determined.[19,40] First, the optogeometrical parameters of the waveguide film were calculated from the baseline (negative t in Figure 2) using the 3-layer mode equation,[19,54,55] resulting in a 170.5 nm thickness (d_F) and 1.7890 refractive index (n_F) for the waveguiding film itself. Inserting these parameters and the measured cover refractive index (n_C) values into the linearized

dx.doi.org/10.1021/ac3034322 | *Anal. Chem.* 2013, 85, 5382−5389

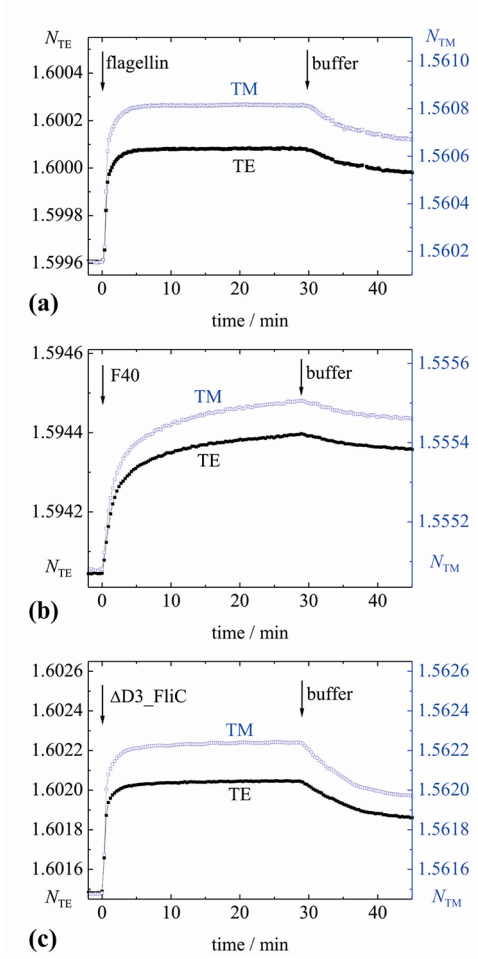

Figure 2. Measured effective refractive indices vs time when 1 mg/mL (a) flagellin, (b) F40, and (c) ΔD3_FliC solution and pure buffer were pumped through the cuvette. The arrows indicate the times when the various solutions reach the spot of measurement in the flow-through cuvette.

homogeneous and isotropic adlayer mode equations[55] the time dependencies of $\tilde{n}_A$ and $\tilde{d}_A$ were calculated, where $\tilde{n}_A$ and $\tilde{d}_A$ are the refractive index and thickness of the adsorbed protein layer respectively assuming a homogeneous and isotropic thin film.[40] These two parameters are the minimum needed to determine the adsorbed mass per unit area based on the equation:[40,56,57]

$$\tilde{M} = \frac{(\tilde{n}_A - n_C)\tilde{d}_A}{dn/dc} \quad (1)$$

where $dn/dc = 0.189$ cm^3/g is the refractive index increment of the flagellin solution.[58]

The results of the calculations are shown in Figure 3 for the three different flagellin variants. It is seen that by removing the terminal regions the protein adsorption significantly slows down and the adsorbed mass decreases to roughly 65%. These features are missing when the central D3 domain was removed. Taken together, these observations suggest that the terminal segments have a central role in governing the adsorption of flagellin on hydrophobic surfaces. Furthermore, the F40 fragment has a much smaller desorption. This is entirely consistent with the adsorbed protein occupying a larger area per molecule (see next section); assuming a constant density

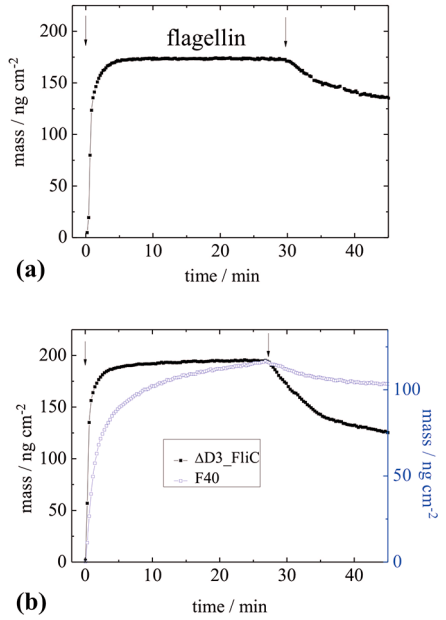

Figure 3. Adsorbed mass per unit area in time for the three different proteins: (a) flagellin, (b) ΔD3_FliC (left axis), and F40 (right axis). The arrows indicate the times when the protein and pure buffer solutions reach the sensing area.

(number per unit area) of attachments, the larger the footprint, the slower the desorption.

Area Occupied Per Adsorbed Protein Molecule. Knowing the molecular weights of each protein ($m_{protein}$) and the adsorbed masses per unit area (M) one can calculate the effective occupied area (f) of a protein molecule, supposing monolayer deposition (which can be inferred from the existence of a plateau despite the strong irreversibility[59]): f[nm^2] = $m_{protein}$[ng]/M[ng/nm^2]. At saturation f = 50.9, 56, and 34 nm^2 for the native flagellin, F40 and ΔD3_FliC, respectively. To estimate the surface coverage these data could be compared with the size of the biomolecules in aqueous solutions. It should be noted that even if the structure of flagellin is known in the flagellar filament (see Figure 4) it is not guaranteed that this conformation is preserved in aqueous solutions. Therefore, only roughly estimated values of the surface coverage can be given. The volume of the protein

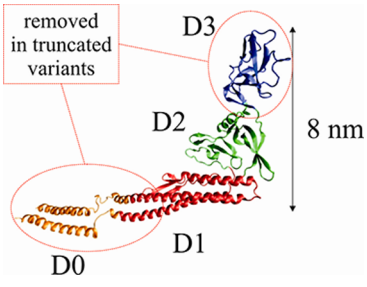

Figure 4. Ribbon diagram representing thestructure of flagellin in the flagellar filament. The protein contains four domains (D0, D1, D2, and D3). In solution the terminal domains D0 and partly D1 are disordered, but the other parts of flagellin form compact, well folded domains. The removed parts of the truncated flagellin variants are also indicated. Both disordered terminal regions are removed in case of F40, while the central D3 domain is removed in ΔD3_FliC. The thickness of the molecule is estimated to be around 2−3 nm.

dx.doi.org/10.1021/ac3034322 | Anal. Chem. 2013, 85, 5382−5389

molecule can be approximated very simply and reliably from the molecular weight of the protein and the average partial specific volume of proteins (around 0.73 cm^3/g).[60] The volumes estimated in this way are 62 nm^3, 48 nm^3 and 51 nm^3 for the flagellin, F40 and ΔD3_FliC, respectively. Assuming that these volumes are tightly packed into boxes and taking the above values of f the surface coverages are estimated to be at least 25−40%. However, these values can be only considered as rough underestimates. Looking also at the dimensions of the proteins in the crystallized state (Figure 4), taking into account their complicated shapes and surfaces a more realistic footprint of the molecules is in the range of 20−30 nm^2. Comparing this with the above f values one can infer that the adsorbed layers are rather close packed with surface coverages in the range of 40−70%.

Pseudoisotropic Adlayer Thickness and Refractive Index. Figure 5 shows the results of the homogeneous and isotropic adlayer model when flagellin and its variants were adsorbed on the hydrophobic waveguide. Several important features can be observed. First, during adsorption of flagellin (Figure 5a) the refractive index of the adlayer reaches a value close to that of the bulk protein solution (n_C = 1.33133), contradicting the close packing inferred previously; at the same time the thickness has values between 15 and 30 nm, with large fluctuations (noise), and which vastly exceeds the averaged (over all possible orientations) size of a single molecule. These discrepancies imply that the homogeneous and isotropic optical layer, model is not valid for the adsorbed flagellin films.

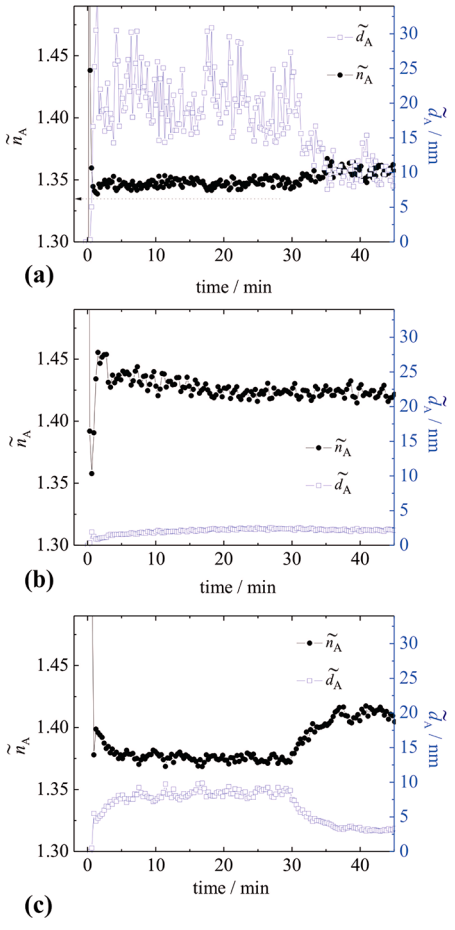

Figure 5. Refractive index and thickness of the adsorbed (a) flagellin, (b) F40, and (c) ΔD3_FliC films calculated from the experimental data shown in Figure 2 using the homogeneous and isotropic thin film model. Note, at the plateau of protein adsorption the calculated refractive index of the flagellin layer is unrealistically low, taking up values very close to that of the bulk solution n_C (indicated by the dashed horizontal arrow). The too large and fluctuating thickness also implies that the homogeneous and isotropic model can not correctly characterize the layer.

On the other hand, the homogeneous and isotropic layer model gives results consistent with a close-packed layer for F40 ($\tilde{n}_A \cong 1.43$, $\tilde{d}_A \cong 2.2$ nm at the plateau of protein adsorption). The averaged layer thickness is reasonable compared to the dimensions of F40; the refractive index also corresponds to an estimated value for protein films in aqueous solutions. The ΔD3_FliC fragment gives significantly lower refractive indices and larger thicknesses ($\tilde{n}_A \cong 1.38$, $\tilde{d}_A \cong 7-10$ nm), also with conspicuous fluctuations, again hinting at an instability in the isotropic layer interpretation.

Even if the homogeneous and isotropic layer model fails to correctly characterize the flagellin and ΔD3_FliC films it can give quite useful information about the structure of the layer.[40] According to Horvath and Ramsden,[40] for a positively birefringent layer the quasi-isotropic refractive index can take up values very close to the refractive index of the cover solution, leading to a singularity in the determined quasi-isotropic thickness. Because of this, the calculated quasi-isotropic thickness will be noisy (see the thickness data in Figure 5a). The large overestimated and noisy thickness data together with the underestimated refractive index obtained from the homogeneous and isotropic adlayer model implies *positive birefringence* ($n_o < n_e$) in the adsorbed flagellin film,[40] which in turn implies that the proteins are not deposited with a random orientation; the molecules have a preferred alignment perpendicular to the surface. This tendency is most pronounced for the complete (intact) flagellin molecule.

Anisotropic Adlayer Model of Adsorbed Protein Layers. In this section we model the investigated protein layers as uniaxially anisosotropic thin films. Such a layer can be characterized by three independent parameters: its thickness (d_A) and its ordinary and extraordinary refractive indices (n_o and n_e). For the adsorbing proteins in the plane of the waveguide there can be no preferred direction, hence $n_x = n_y = n_o$ and $n_z = n_e$. The layer is thin compared to the wavelength of the light ($d_A \ll \lambda$), since we have inferred from the saturation of M that at most one monolayer is adsorbed for each variant. Such a uniaxially anisotropic thin layer perturbs the effective refractive indices of the modes propagating in the 3-layer waveguide (along the guide without the adsorbed film). The mode equations can be written in the following form, where Δd_F is the perturbation term due to the thin uniaxial adlayer.[35,40,55,61]

$$\pi m \cong \frac{2\pi}{\lambda}\sqrt{n_F^2 - N^2}\,(d_F + \Delta d_F) - \arctan\left[\left(\frac{n_F}{n_C}\right)^{2\rho}\frac{\sqrt{N^2 - n_C^2}}{\sqrt{n_F^2 - N^2}}\right] - \arctan\left[\left(\frac{n_F}{n_S}\right)^{2\rho}\frac{\sqrt{N^2 - n_S^2}}{\sqrt{n_F^2 - N^2}}\right] \quad (2a)$$

and

dx.doi.org/10.1021/ac3034322 | Anal. Chem. 2013, 85, 5382−5389

$$\Delta d_F = \frac{n_o^2 - n_C^2}{n_F^2 - n_C^2}\left[\frac{\left(\frac{N}{n_C}\right)^2 + \left(\frac{N}{\tilde{n}}\right)^2 - 1}{\left(\frac{N}{n_C}\right)^2 + \left(\frac{N}{n_F}\right)^2 - 1}\right]^{\rho} d_A \quad (2b)$$

$$\tilde{n}^2 = n_o^2\left[\frac{1 - \frac{n_C^2}{n_o^2}}{1 - \frac{n_C^2}{n_e^2}}\right] \quad (2c)$$

N is the effective refractive index of the propagating waveguide mode, m = 0, 1, 2,... is the mode order, and ρ = 0 for the transverse electric (TE) modes and ρ = 1 for the transverse magnetic (TM) modes; n_F and d_F are the refractive index and thickness of the waveguiding layer; n_C and n_S are the refractive indices of the aqueous cover medium and waveguide support, respectively.

The adsorbed thin layer increases the effective refractive indices of the waveguide modes and the shift is different for the TE and TM modes ($\Delta N_{TE} \neq \Delta N_{TM}$).[40] These effective refractive index shifts due to the adlayer can be precisely followed by the OWLS technique (see Figure 2). However, from the independently measured two effective refractive index values it is impossible to calculate the three independent optogeometrical parameters of the uniaxial adlayer. To solve the above equations and calculate the optogeometrical parameters of the adsorbed layer (n_o, n_e, and d_A) from the measured effective refractive indices we fixed the averaged refractive index of the adsorbed films. This approximation, to mathematically treat self-assembling anisotropic layers when only two effective refractive indices are measured, was previously applied for giant glycoptroteins spread on a hydrophobic waveguide surface.[41]

This assumption is grounded in the fact that OWLS averages over the approximately 1 mm^2 incoupling grating area illuminated by the laser light. It was previously shown using numerical simulations that when the waveguide surface is partially covered by discrete objects the OWLS technique surface-averages the different effective refractive indices of the propagating waveguide mode (where the objects are and where they are not).[62] This averaging leads to the following equation for the measured effective refractive index shifts for a partially covered surface: $\Delta N = \theta \Delta N_{object}$, where θ is the surface coverage and ΔN_{object} is the local effective refractive index shift at the homogeneously covered areas. Using this equation for the TE and TM modes and the formulas for ΔN in ref **41** it is easy to show that the determined refractive indices (n_o and n_e) for the anisotropic film are those of the objects and the layer thickness is necessarily a surface-averaged value between the covered and uncovered areas, that is, $d_A = \theta d_{object}$.

Building on the above results, in further calculations we fixed the averaged refractive index at a reasonable value of $\bar{n}_A$ = 1.43. This is the value measured for the isotropic F40 layer (since the 3 variants are compositionally very similar we can assume that the intrinsic averaged refractive index is the same for all 3 cases). With this assumption, together with the additional equation[39,40,41]

$$\bar{n}_A^2 = (2n_o^2 + n_e^2)/3 \quad (3)$$

the three independent parameters characterizing the uniaxial adlayer can then be determined for all of the data shown in Figure 3.

The results are plotted in Figure 6. The calculations, as expected from the quasi-isotropic analysis, revealed a significant

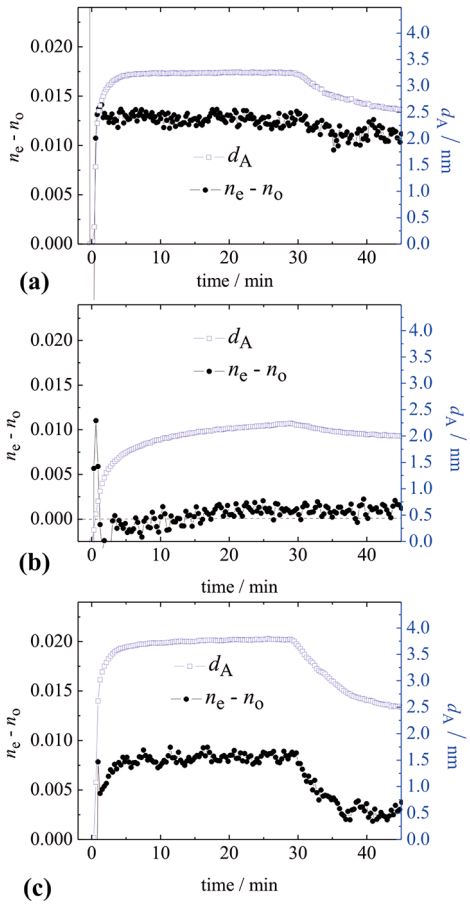

Figure 6. Birefringences and thicknesses of the adsorbed layers treating them as uniaxially anisotropic. (a) flagellin, (b) F40, and (c) ΔD3_FliC.

positive birefringence ($n_o < n_e$) in the flagellin layer reaching a value of 0.0125 at the plateau of the adsorption (see Figure 6a). At this point the calculated thickness of the film is around 3.25 nm. For comparison, the birefringence observed in black lipid membranes using CPWR is around 0.05[27] and for supported lipid bilayer membranes made by vesicle rupture and measured using DPI is around 0.02.letele

Several important features can be observed by looking at the change in layer thickness and birefringence in time (Figure 6). Both have their maximum values at the plateau of protein adsorption. It is reasonable that the ordering of the molecules is most pronounced when the layer is closely packed. As the surface coverage decreases the thickness of the layer also decreases. The behavior is in full agreement with the above model, since decreasing surface coverage means decreasing averaged thickness.

It should be emphasized that only when assuming an unrealistically low averaged refractive index (very close to that of the refractive index of water) we obtain zero birefringence for flagellin, but in this case the calculated layer thickness is far too large compared to the dimensions of the molecule. We note that the birefringence is also present when, as an alternative approximation, the averaged layer thickness is fixed during the calculations. It should be, however, emphasized that the investigated molecules are quite asymmetric, therefore the

dx.doi.org/10.1021/ac3034322 | Anal. Chem. 2013, 85, 5382−5389

choice of fixed layer thickness is quite arbitrary. For example, by fixing the layer thickness at a value of 4−5 nm, corresponding to the estimated averaged size of flagellin, the refractive indices calculated from the TE and TM mode equations differ by around 0.008. For all reasonable averaged refractive indices and thicknesses, the birefringence is present.

Figure 7 shows how flagellin might have a preferred adsorption orientation at the surface. The fact that the removal of the disordered terminal regions significantly slows down the adsorption suggests that flagellin preferentially adsorbs on hydrophobic surfaces through the terminal regions involved in the D0 domain in the polymeric form (see Figure 7 for a schematic illustration). This is also in full agreement with the structural features of the D0 domain. This domain contains a significant number of surface-exposed hydrophobic residues,[49] which presumably interact with hydrophobic surfaces, facilitating the adsorption. (Hydrophobic interaction between the D0 domains of flagellin subunits plays an essential role in the formation of the inner core of flagellar filaments.[47])

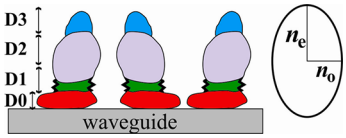

Figure 7. Schematic illustration of the preferred orientation of the adsorbed flagellin molecules on the hydrophobic waveguide. The refractive index ellipsoid is also shown (at right). It is proposed that flagellin adsorbs to the nonpolar surface through its disordered terminal segments forming the D0 domain in the filamentous form (red in color). The terminal parts of the D1 domain are also disordered in solution[33,36] (green in color).

In contrast to the intact flagellin layer, no birefringence was observed in the film of F40 (in which the terminal regions are removed) (see Figure 6b). This is in agreement with the above findings for the flagellin; without the terminal regions the molecule no longer has a part with a significant ratio of surface-exposed hydrophobic residues. It is also revealing to investigate the data obtained for the ΔD3_FliC variant. In this case the terminal regions are present, but the central D3 domain is removed. Again, a significant positive birefringence was observed, supporting our hypothesis about the role of the terminal domains in adsorption.

Our results, therefore, suggest that the same forces playing a role in the self-assembly of the flagellins into the flagellar filaments govern the adsorption of the flagellin on hydrophobic surfaces. It is a kind of structural adaptation to maximize the number of hydrophobic contacts. We can compare this with what is observed for compact globular proteins like serum albumin, which denature on hydrophobic surfaces, losing their compact globular structure in order to contact their hydrophobic internal cores with the surface, in accord with the thermodynamic theory.[63,64]

■ CONCLUSIONS AND OUTLOOK

In summary, the surface adsorption of flagellin and its truncated variants was followed using OWLS. The adsorption process of the molecules was monitored in real time without using any labeling. No significant adsorption was detected on hydrophilic surfaces, suggesting that strong hydrophilic repulsion[65] is sufficient to overcome the attractive components of any interfacial interaction. It was found that by removing the terminal segments of flagellin the protein adsorption significantly slows down on hydrophobic surfaces, suggesting that the disordered terminal regions have a central role in the surface adsorption process, which is in agreement with the structure of the D0 domain of polymeric flagellin, which contains a substantial amount of surface-exposed hydrophobic residues.

Moreover, the waveguides employed supported two modes with different polarizations making it possible (i) to determine the adsorbed layer thickness and refractive index using a homogeneous and isotropic layer model and (ii) by fixing the averaged refractive index of the films to model the layers as uniaxially anisotropic. In the second case, we determined the optical birefringence of the adsorbed films. It was found that the homogeneous and isotropic layer model failed to correctly characterize the flagellin and ΔD3_FliC (central D3 domain is removed) films, but gave reasonable results for the F40 (D0 and some parts of the D1 domain are removed) layer. The anisotropic modeling revealed a significant *positive birefringence* ($n_o < n_e$) in the flagellin and ΔD3_FliC films, but no birefringence for F40. All of these findings suggested oriented adsorption of flagellin and ΔD3_FliC. We concluded that these proteins adsorb on hydrophobic surfaces through their terminal segments.

We believe that these results open up new perspectives in several directions. They emphasize the importance of developing appropriate and reliable optical theories to model the optical properties of films assembled from nanometer-scale isotropic and inhomogeneous objects. The orientations of individual bonds and secondary structures inside the film can also have an importance and should be theoretically treated. The need for the development of multimodal and label-free techniques is also emphasized by the present study.

The results presented can find also applications in nanobiotechnology. Substituting the central D3 domain by an appropriate artificial peptide sequence can give flagellin analyte affinity sensing or enzymatic properties.[52,53,58] Recently, the incorporation of green fluorescent protein (GFP) was also demonstrated.[66] The easy formation of compact, stable, well ordered and oriented functional layers can facilitate the development of these directions.

■ AUTHOR INFORMATION

Corresponding Author

*E-mail: horvathr@mfa.kfki.hu.

Notes

The authors declare no competing financial interest.

■ ACKNOWLEDGMENTS

Robert Horvath gratefully acknowledges a Reintegration Marie Curie Fellowship from the European Commission and a Fellowship from the Hungarian Scientific Research Fund (OTKA PD). This work was supported by the National Development Agency grants TÁMOP-4.2.2/B-10/1-2010-0025 and REG_KD_09-2-2009-0022-NANOFLAG and by the "Lendület" program of the Hungarian Academy of Sciences.

■ REFERENCES

(1) Ramsden, J. J. *Biomedical Surfaces*; Artech House: Norwood, MA, 2008.

(2) Malmsten, M., Ed. *Biopolymers at Interfaces*, 2nd ed; Dekker: New York, 2003.

(3) Dejardin, Ph., Ed. *Proteins at Solid–Liquid Interfaces*; Springer-Verlag: Heidelberg, Germany, 2006.
(4) Ramsden, J.J. Q. *Rev. Biophys.* **1994**, *27*, 41–105.
(5) Cooper, M. A. *Nat. Rev. Drug Discovery* **2002**, *1*, 515–528.
(6) Fang, Y. *Drug Discovery Today Technol.* **2010**, *7*, e5–e11.
(7) Ramsden, J. J.; Horvath, R. *J. Recept. Signal Transduction Res.* **2009**, *29*, 211–223.
(8) Tollin, G.; Salamon, Z.; Hruby, V. J. *Trends Pharmacol. Sci.* **2003**, *24*, 655–659.
(9) Mendes, S. B; Saavedra, S. S. *Opt. Express* **1999**, *4*, 449–456.
(10) Runge, A. F.; Rasmussen, N. C.; Saavedra, S. S.; Mendes, S. B. *J. Phys. Chem. B.* **2005**, *109*, 424–431.
(11) Fan, X.; White, I. M.; Shopova, S. I.; Zhu, H.; Suter, J. D.; Sun, Y. *Anal. Chim. Acta* **2008**, *620*, 8–26.
(12) Schmitt, K.; Schirmer, B.; Hoffmann, C.; Brandenburg, A.; Meyrueis, P. *Biosens. Bioelectron.* **2006**, *22*, 2591–2597.
(13) Hunt, H. K.; Armani, A. M. *Nanoscale* **2010**, *2*, 1544–1559.
(14) Homola, J.; Yee, S. S.; Gauglitz, G. *Sensors Actuators B* **1999**, *54*, 3–15.
(15) Kozma, P.; Hamori, A.; Kurunczi, S.; Cottier, K.; Horvath, R. *Sensors Actuators B* **2011**, *155*, 446–450.
(16) Patko, D.; Cottier, K.; Hamori, A.; Horvath, R. *Opt. Express* **2012**, *20*, 23162–23173.
(17) Armani, A. M.; Kulkarni, R. P.; Fraser, S. E.; Flagan, R. C.; Vahala, K. J. *Science* **2007**, *317*, 783–787.
(18) Ramsden, J. J. High Resolution Molecular Microscopy. In *Proteins at Solid–Liquid Interfaces*; Dejardin, Ph., Ed.; Springer-Verlag: Heidelberg, Germany, 2006; pp 23–49.
(19) Ramsden, J. J. *J. Stat. Phys.* **1993**, *73*, 853–877.
(20) Ramsden, J. J. Kinetics of Protein Adsorption. In *Biopolymers at Interfaces*; Malmsten, M., Ed.; Dekker: New York, 1998; Chapter 10, pp 321–361.
(21) Calonder, C.; Van Tassel, P. R. *Langmuir* **2001**, *17*, 4392–4395.
(22) Mendes, S. B.; Bradshaw, J. T.; Saavedra, S. S. *Appl. Opt.* **2004**, *43*, 70–78.
(23) Mendes, S. B.; Saavedra, S. S. *Appl. Opt.* **2000**, *39*, 612–621.
(24) Runge, A. F.; Saavedra, S. S; Mendes, S. B.. *J. Phys. Chem. B.* **2006**, *110*, 6721–6731.
(25) Runge, A. F.; Mendes, S. B.; Saavedra, S. S. *J. Phys. Chem. B* **2006**, *110*, 6732–6739.
(26) Du, Y. Z.; Saavedra, S. S. *Langmuir* **2003**, *19*, 6443–6448.
(27) Salamon, Z.; Tollin, G. *Biophys. J.* **2001**, *80*, 1557–1567.
(28) Salamon, Z.; Brown, M. F.; Tollin, G. *Trends Biochem. Sci.* **1999**, *24*, 213–219.
(29) Salamon, Z.; Macleod, H. A.; Tollin, G. *Biophys. J.* **1997**, *73*, 2791–2797.
(30) Salamon, Z.; Tollin, G.; Alves, I.; Hruby, V. Plasmon Resonance Methods in Membrane Protein Biology: Applications to GPCR Signaling. *Methods in Enzymology,* ; Elsevier: Amsterdam, 2009, Vol. *461*, Chapter 6 , pp 123–146.
(31) Noinville, S.; Bruston, F.; El, A. C.; Baron, D.; Nicolas, P. *Biophys. J.* **2003**, *85*, 1196–206.
(32) Ramsden, J. J. *J. Stat. Phys.* **1993**, *73*, 853–877.
(33) Picart, C.; Gergely, C.; Arntz, Y.; Voegel, J. C.; Schaaf, P.; Cuisinier, F. J. G.; Senger, B. *Biosens. Bioelectron.* **2004**, *20*, 553–561.
(34) Mann, E. K. *Langmuir* **2001**, *17*, 5872–5881.
(35) Horvath, R.; Fricsovszky, G.; Papp, E. *Biosens. Bioelectron.* **2003**, *18*, 415–428.
(36) Horvath, R.; Cottier, K.; Pedersen, H. C.; Ramsden, J. J. *Biosens. Bioelectron.* **2008**, *24*, 799–804.
(37) Mann, E. K.; Heinrich, L.; Schaaf, P. *Langmuir* **1997**, *13*, 4906–4909.
(38) Calonder, C.; Talbot, J.; Ramsden, J. J. *J. Phys. Chem. B* **2001**, *105*, 725–729.
(39) Ramsden, J. J. *Philos. Mag. B.* **1999**, *79*, 381–386.
(40) Horvath, R.; Ramsden, J. J. *Langmuir* **2007**, *23*, 9330–9334.
(41) Horvath, R.; McColl, J.; Yakubov, G. E.; Ramsden, J. J. *J. Chem. Phys.* **2008**, *129*, 071102.
(42) Yakubov, G. E.; McColl, J.; Bongaerts, J. H. H.; Ramsden, J. J. *Langmuir* **2009**, *25*, 2313–2321.
(43) Coles, J. M.; Chang, D. P.; Zauscher, S. *Curr. Opin. Colloid Interface Sci.* **2010**, *15*, 406–416.
(44) Vonderviszt, F.; Namba, K. Structure, Function and Assembly of Flagellar Axial Proteins. In *Fibrous Proteins*; Scheibel, T., Ed.; Landes Biosciences: Austin, TX, 2008; pp 58–76.
(45) Vonderviszt, F.; Uedaira, H.; Kidokoro, S.; Namba, K. *J. Mol. Biol.* **1990**, *214*, 97–104.
(46) Vonderviszt, F.; Kanto, S.; Aizawa, S. I.; Namba, K. *J. Mol. Biol.* **1989**, *8*, 127–133.
(47) Aizawa, S. I.; Vonderviszt, F.; Ishima, R.; Akasaka, K. *J. Mol. Biol.* **1990**, *211*, 673–677.
(48) Vonderviszt, F.; Aizawa, S. I.; Namba, K. *J. Mol. Biol.* **1991**, *221*, 1461–1474.
(49) Yonekura, K.; Maki-Yonekura, S.; Namba, K. *Nature* **2003**, *424*, 643–650.
(50) Samatey, F. A.; Imada, K.; Nagashima, S.; Vonderviszt, F.; Kumasaka, T.; Yamamoto, M.; Namba, K. *Nature* **2001**, *410*, 331–337.
(51) Muskotál, A.; Seregélyes, C.; Sebestyén, A.; Vonderviszt, F. *J. Mol. Biol.* **2010**, *403*, 607–615.
(52) Szabó, V.; Muskotál, A.; Tóth, B.; Mihovilovic, M. D.; Vonderviszt, F. *PLoS One* **2011**, *6*, No. e25388.
(53) Kumara, M. T.; Tripp, B. C.; Muralidharan, S. *Biomacromolecules* **2007**, *8*, 3718–3722.
(54) Tien, P. *Rev. Mod. Phys.* **1977**, *49*, 361–420.
(55) Tiefenthaler, K.; Lukosz, W. *J. Opt. Soc. Am. B.* **1989**, *6*, 209–220.
(56) De Feijter, J. A.; Benjamins, J.; Veer, F. A. *Biopolymers* **1978**, *17*, 1759–1772.
(57) Ball, V.; Ramsden, J. J. *Biopolymers* **1998**, *46*, 489–492.
(58) Kurunczi, S.; Horvath, R.; Yeh, Y. P.; Muskotál, A.; Sebestyén, A.; Vonderviszt, F.; Ramsden, J. J. *J. Chem. Phys.* **2009**, *130*, 011101.
(59) Ramsden, J. J. *Biopolymers* **1993**, *33*, 475–477.
(60) Tsai, J.; Taylor, R.; Chothia, C.; Gerstein, M. *J. Mol. Biol.* **1999**, *290*, 253–266.
(61) Lukosz, W. *Biosens. Bioelectron.* **1997**, *12*, 175–184.
(62) Cottier, K.; Horvath, R. *Appl. Phys. B: Lasers Opt.* **2008**, *91*, 319–327.
(63) Fernández, A.; Ramsden, J. J. *J. Biol. Phys. Chem.* **2001**, *1*, 81–84.
(64) Aggarwal, N.; Lawson, K.; Kershaw, M.; Horvath, R.; Ramsden, J. J. *Appl. Phys. Lett.* **2009**, *94*, 083110.
(65) Van Oss, C. J. *Forces Interfaciales en Milieux Aqueux*; Masson: Paris, 1996.
(66) Klein, A.; Toth, B.; Jankovics, H.; Muskotal, A.; Vonderviszt, F. *Protein Eng., Des. Sel.* **2012**, *25*, 153–157.